energies

MDPI

Review

Combined Methane Pyrolysis and Solid Carbon Gasification for Electrified CO_2-Free Hydrogen and Syngas Production

Patrice Perreault [1,2,3,*], Cristian-Renato Boruntea [3], Heena Dhawan Yadav [3], Iria Portela Soliño [3] and Nithin B. Kummamuru [1,3]

[1] Laboratory for the Electrification of Chemical Processes and Hydrogen (ElectrifHy), University of Antwerp, Olieweg 97, 2020 Antwerp, Belgium
[2] Blue App, Olieweg 97, 2020 Antwerp, Belgium
[3] Sustainable Energy, Air and Water Technology, Department of Bioscience Engineering, University of Antwerp, Groenenborgerlaan 171, 2020 Antwerp, Belgium
* Correspondence: patrice.perreault@uantwerpen.be

Abstract: The coupling of methane pyrolysis with the gasification of a solid carbon byproduct provides CO_2-free hydrogen and hydrogen-rich syngas, eliminating the conundrum of carbon utilization. Firstly, the various types of carbon that are known to result during the pyrolysis process and their dependencies on the reaction conditions for catalytic and noncatalytic systems are summarized. The synchronization of the reactions' kinetics is considered to be of paramount importance for efficient performance. This translates to the necessity of finding suitable reaction conditions, carbon reactivities, and catalysts that might enable control over competing reactions through the manipulation of the reaction rates. As a consequence, the reaction kinetics of methane pyrolysis is then emphasized, followed by the particularities of carbon deposition and the kinetics of carbon gasification. Given the urgency in finding suitable solutions for decarbonizing the energy sector and the limited information on the gasification of pyrolytic carbon, more research is needed and encouraged in this area. In order to provide CO_2-free hydrogen production, the reaction heat should also be provided without CO_2. Electrification is one of the solutions, provided that low-carbon sources are used to generate the electricity. Power-to-heat, i.e., where electricity is used for heating, represents the first step for the chemical industry.

Keywords: methane pyrolysis; solid carbon gasification; CO_2-free hydrogen production; electrification; power-to-heat

Citation: Perreault, P.; Boruntea, C.-R.; Dhawan Yadav, H.; Portela Soliño, I.; Kummamuru, N.B. Combined Methane Pyrolysis and Solid Carbon Gasification for Electrified CO_2-Free Hydrogen and Syngas Production. *Energies* **2023**, *16*, 7316. https://doi.org/10.3390/en16217316

Academic Editors: Muhammad Aziz and Vladislav A. Sadykov

Received: 21 September 2023
Revised: 20 October 2023
Accepted: 27 October 2023
Published: 28 October 2023

1. Introduction

Hydrogen (H_2) is currently seen as a key element for enabling a sustainable and environmentally friendly energy source. It provides the answer to one of the most urgent problems nowadays: the heavy emission of greenhouse gases (GHGs) from the processing of fossil fuels and their scarcity in the near future. Global H_2 production is currently dominated by steam methane reforming (SMR), which, based on 2019 reports, accounts for 76% of the total amount produced, followed by coal gasification with 23%, and electrolysis with 2% [1]. CO_2 emissions resulting from the production of H_2 via the current state-of-the-art SMR are estimated to be 9–12 kg CO_2/kg H_2, i.e., both due to the reaction and the energy requirements [2] (Figure 1). On the usage side, global H_2 consumption is divided as follows: 33% for oil refining, 27% for ammonia production, 11% for methanol synthesis, and 3% goes into iron manufacturing [1]. The amount of H_2 required for ammonia production is particularly interesting as it is estimated that approximately 48% of the global population is fed by synthetic ammonia [3]. It deserves mentioning that even though large quantities of ammonia are produced and the transportation routes are well established worldwide, it would be challenging to divert part of the ammonia produced for H_2 applications, without

perturbating the value chain, for example, due to the recent surge of interest in ammonia cracking from the industrial sector [4].

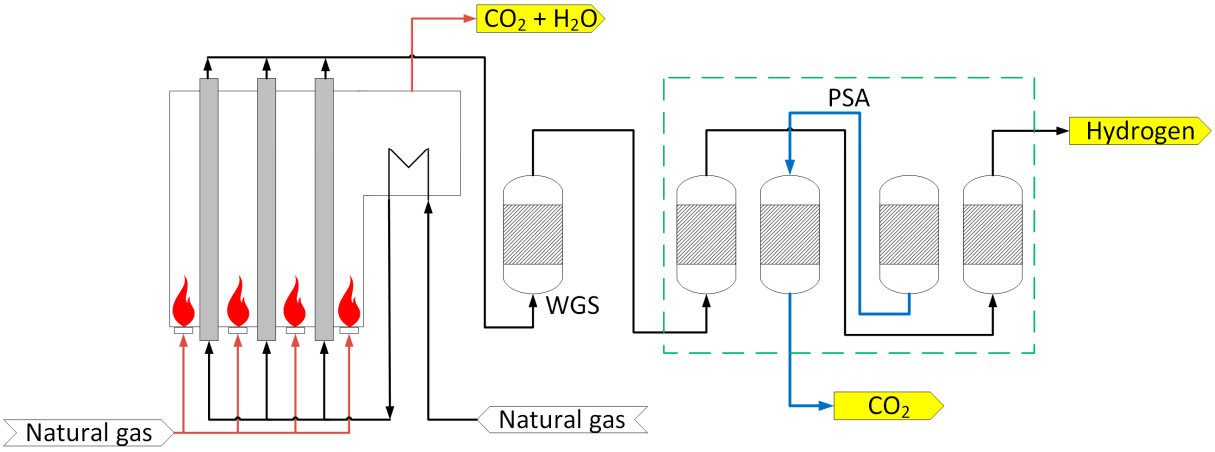

Figure 1. Hydrogen based on the reformer technology, highlighting the CO_2 emitted from both the energy requirements (red line) and reaction (blue line). Natural gas is used both to fire the methane burners and as a feed for the reaction, after being preheated in the convection section. The hydrogen content is increased in the water gas shift (WGS) reactor, and CO_2 is removed by pressure swing adsorption (PSA).

Many methods for H_2 production have been investigated in the literature and industry, described by color codes ranging from green (via water electrolysis with renewable energy input and no CO_2 emissions) to black (via thermochemical splitting of water with coal as an energy source and high CO_2 emissions) [5]. Each method has been evaluated based on the following characteristics: H_2 source (e.g., water, natural gas, or biomethane), energy source (e.g., renewable, grid electricity, nuclear, etc.), production process (e.g., electrolysis and thermochemical, etc.), byproduct (O_2, CO_2, solid carbon, etc.), and values for CO_2 emissions per ton of H_2 produced. We acknowledge the fact that although H_2 produced via water electrolysis with renewable energy (e.g., offshore wind energy) input is labeled as green with no CO_2 emissions along the production chain, some offshore wind platforms have diesel generators installed for specific operational needs, such as during commissioning. Recently, the concept of "golden hydrogen" has been put forward by Lubbe et al. [6] for H_2 produced in dedicated solar generators.

A cleaner and more sustainable alternative to SMR must be developed, and ideally, already at an industrially relevant size. Methane pyrolysis is a thermal and/or thermocatalytic process where methane is split, ideally, into H_2 gas and solid carbon, in the absence of CO_2 emissions. This alternative to SMR yields hydrogen that is labeled between blue and green hydrogen, i.e., turquoise hydrogen. While relying on methane as a feedstock (similar to grey and blue hydrogen), if the source of electricity fueling the process is renewable, the process is zero-net carbon, and even carbon negative if the source of methane is also renewable (e.g., biogas or biomethane) [7].

Biogas from anaerobic digestion (AD) from organic waste material has a huge potential as a CH_4 feedstock, especially in Europe, where the installation of AD has boomed during the past few decades due to legal and financial incentives [8]. While renewable, the strategy to convert biogas into biomethane requires an expensive upgrade step. Raw contains methane (50–80%), carbon dioxide (20–50%), water (saturated), as well as minor impurities such as N_2, NH_3, and H_2S. To reach pipeline quality standards, the methane content must be increased to over 96%. CO_2 is removed via either physical and chemical CO_2 absorption, pressure swing adsorption (PSA) and vacuum swing adsorption (VSA), membrane separation, cryogenic separation, and/or biological methane enrichment [9]. Considering the 2018 prices of natural gas, it was estimated then that up to 30 € MWh^{-1} (or 150 € ton^{-1} biogas) in incentives was needed for the grid injection of upgraded biomethane [8]. In

small installations, biogas is instead used for on-site combined heat and power (CHP) productions at a low efficiency.

A better option would be to convert it to H_2 at a minimal energy cost. Verbeeck et al. [8] demonstrated that sorption-enhanced steam biomethane reforming to produce H_2 is uneconomical due to (i) the extra cost of biomethane upgrading, (ii) the energy requirements for the SMR reaction (206 kJ mol^{-1} standard enthalpy), and (iii) the further separation/purification of H_2. CH_4 pyrolysis is the least energy-intensive CH_4-to-H_2 conversion route (75 kJ mol^{-1} standard enthalpy, i.e., approximately one-third of that of SMR) [10]. However, the market cannot absorb all the carbon produced alongside the hydrogen during methane pyrolysis [11–13]. The solid carbon and the CO_2 should instead serve as a reagent for CO synthesis. Recent developments in thermal CH_4 pyrolysis can thus lead to "green", CO_2-free low-cost H_2. However, since the starting material is not pure CH_4 but biogas, the produced H_2 has to be separated from the unconverted CH_4, CO_2, and potentially CO and C_2s due to the nonoxidative coupling of CH_4. Luckily, in light of recent research results, a single-step H_2 storage/purification at mild conditions could be envisioned using liquid organic hydrogen carriers (LOHCs) due to the high selectivity of LOHCs for H_2, if, however, the extent of methanation can be limited [14,15]. LOHCs are normally envisioned to be used as H_2 carriers: H_2 is stored at 30–50 bars and 150–300 °C via a catalytic exothermic reaction by saturating the double bonds of organic molecules, followed by an endothermic catalytic dehydrogenation reaction. The three most-studied LOHC molecules systems are methylcyclohexane (MCH)-toluene, H12-N-ethyl carbazole/N-ethyl carbazole (NEC), and perhydro dibenzyltoluene/dibenzyltoluene (DBT). The high carcinogenicity of toluene, coupled with the low boiling points of both components and the high dehydrogenation enthalpy (68 kJ mol^{-1} H_2), excludes the MCH/toluene system as a viable option, even though it has the highest theoretical gravimetric storage capacity (7.2 wt.%). For the H12-NEC/NEC system, even though it possesses the lowest dehydrogenation enthalpy (51 kJ mol^{-1} H_2), the fact that both forms are solid at ambient conditions limits their practical implementation. Finally, DBT combines a large availability, low toxicity (not classified as a dangerous substance in Europe), adequate melting and boiling points, and the possibility of using the existing infrastructure for fossil fuel, e.g., making use of tanker ships, rail trucks, road tankers, and tank farms [16]. Jorschick et al. [14] extended the potential use of LOHCs by showing that alumina-supported Rh and Pd catalysts hydrogenate DBT in the presence of CO and CO_2, with a low-to-moderate selectivity toward methanation. They also showed that the H_2 released was 99.99% pure [15].

On the other hand, carbon gasification is an established process for the production of CO and synthesis gas, where synthesis gas can be obtained with a ratio varying from 1 to 3 [17]. Interestingly, although various types of carbon have made the subject of various kinetic gasification studies [18–25] and reviews [26], the gasification of pyrolytic carbon has seldomly been addressed [17,27].

The observed decrease in the catalyst activity for catalytic methane decomposition (CMD) with time on stream, due to catalytically inactive carbon species (e.g., graphitic carbon with its limited reactivity [28]) depositing on catalysts, represents a challenge that can be tackled in a number of ways, e.g., the development of a "coke-resistant" catalyst represents one potential approach, which has raised a lot of attention recently in the context of the nonoxidative coupling of methane (NOCM) into olefins [29–32], including the use of single-atom Fe catalysts [33]. However, from these results, one has to expect that coke formation is inevitable and the absence of coking seems hardly realizable. Instead, the aim should be to limit it as much as possible. Another interesting approach, not yet investigated up to now based on the authors' knowledge, consists of designing a process combining methane pyrolysis and carbon gasification, i.e., taking advantage of the presence of CO_2 (and water) in the biogas to catalytically gasify the coke, ideally leading to a "net zero coking rate". This approach would, however, only make sense if we can show that both processes present a compatible window of operation, both in terms of the operating conditions and with respect to the catalysts used. Although various methods for the valorization

of carbon byproducts have already been summarized in the literature [34], there is still a high demand for finding suitable solutions to this important issue. In this review, we aim to emphasize the benefits of simultaneous methane pyrolysis and carbon gasification to stimulate scientific research in this area. Firstly, we address the reaction kinetics of methane pyrolysis, the current status of electrified processes for minimum CO_2 emissions, followed by the kinetics of solid carbon gasification.

2. Methane Pyrolysis

The abundance of natural gas reserves and biomethane makes pyrolysis an important intermediate step toward greener H_2 production technologies. The reaction of methane decomposition is endothermic in nature and is favored above 500 °C using metal-based catalysts [35]. Methane is a nonpolar highly symmetric molecule with a net-zero dipole moment, and as a consequence, activation of the CH_3–H bond is difficult to take place and still represents one of the greatest challenges in catalysis. Moreover, because splitting the C–H bond leads to the production of a tertiary carbon, it has a very high dissociation energy (approximately 435 kJ/mol) [36], which makes methane pyrolysis a highly temperature-intensive process, and justifies the need for efficient catalysts. Carbon formation during methane pyrolysis constitutes one of the bottlenecks for industrial production, especially in reducing the economic gap with other H_2 production technologies. Thermal decomposition of methane takes place at high temperatures, flooding the reactor with carbon product. Moreover, carbon deposition is known to increase with temperature, posing several difficulties for its removal, which otherwise deactivates the catalyst [37]. Although the regeneration of metal catalysts is a viable method to remove carbon from its surface, CO_2 is produced in this process, hindering the environmental advantage of methane pyrolysis. Decoking with air can lead to hot spots and contribute to the loss of dispersion of the active metal.

2.1. Reaction Kinetics

In order to explore the feasibility of the proposed combined approach of methane pyrolysis and pyrolytic coke gasification, we purposely focus in this section on the kinetics of CMD in gas–solid systems. We thus did not consider the available kinetic characterization in molten salts [38,39], plasma [40–42], and only briefly reviewed the kinetics of thermal decomposition for the sake of providing a reliable portrait of gas–solid CMD with homogeneous gas-phase radical-based chemistry occurring in the gas phase of this high-temperature process. The distinction between thermal and catalytic decomposition in the literature is sometimes blurred as some researchers investigated the catalytic effect of the reactor walls during thermal decomposition. We decided to only review the articles where catalysts were purposely used, and where the catalyst deactivation was considered. Interestingly, although there are a significant number of articles focusing on catalyst development and their characterization, there is a notable scarcity of the literature concerning the kinetic characterization aspect.

The overall mechanism of CMD is composed of methane adsorption either molecularly or dissociatively [43], and the desorption of hydrogen is assumed to be the rate-limiting step [44]. The sequential dehydrogenation reactions of the adsorbed species ($CH_4^* \rightarrow CH_3^* \rightarrow CH_2^* \rightarrow CH^*$) result in the formation of solid carbon (Figure 2). In fact, the kinetics of CMD is plainly part of the SMR reaction mechanism, i.e., up to the point where the adsorbed oxygen starts to interact with adsorbed CH_n* species, minimizing coke formation in the case of SMR.

The methane pyrolysis reaction rate is often expressed as a power law kinetic model, both for CMD and noncatalytic thermal methane decomposition (Equation (1)) [45,46].

$$r = k \cdot P_{CH4}^{n} \quad (1)$$

The main disadvantage of this model is of course the absence of information on the reaction mechanism as well as the evolution of the catalytic surface and loss of activity due

to coke formation: its use for reactor design and simulation predicts unrealistic continuous H_2 production for an infinite amount of time. The use of activity functions is well known to account for the loss of activity, but they are often based on time [47] instead of the surface coke. The former strategy allows of course for easier data collection but offers little information on the catalyst and is dependent on the reactor and experimental conditions used. On top of that, time-based deactivation functions more or less accurately describe the actual deactivation over time (c.f., in [47]).

More complete approaches should consider minimally the chemical equilibrium and the reverse reaction, as well as deactivation functions applied to the initial reaction rates [48], a kinetic model of carbon deposition [49], etc. The optimal solution, especially for the optimization of reactors, would be the development of microkinetic models, which was performed for edge-decorated nanocarbons catalysts [50], as well as for Ni/SiO_2 catalysts [43].

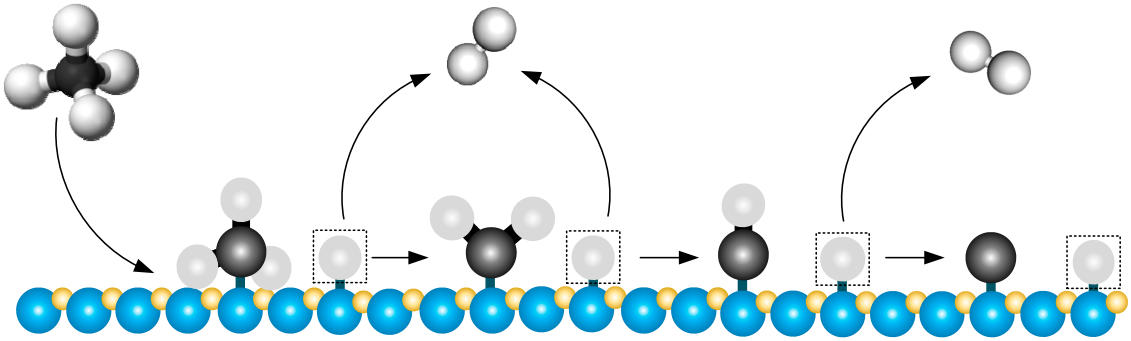

Figure 2. Catalytic methane decomposition reaction mechanism over an ideal generic catalytic surface.

2.1.1. Carbon-Based Catalysts

Muradov [51] proposed a kinetic model for carbon-based catalysts accounting for the blockage of the active sites by carbon species, and the simultaneous increase in the rate of methane pyrolysis for catalytically active formed carbon species. Interestingly, as the formation of coke at the surface increases with time on stream, the performance of all carbon-based catalysts might only differ in the initial stages of CMD, i.e., until the point where the carbon-based catalysts are fully covered in pyrolytic carbon [50].

Trommer et al. [52] characterized the kinetics of methane decomposition in a high flux solar concentrator co-fed with 10 mm of activated carbon (900 m^2/g BET) particles. They proposed an initial nondissociative adsorption of methane, followed by the pyrolysis of the adsorbed species. The activation for the reaction step varied between 147 and 162 kJ/mol, following the nature of the reactor model used (plug or mixed flow). Zhou et al. modeled the CMD using a 0.5 order power law between 1023 and 1173 K on activated carbon obtained from coconut shells and coal. Dahl et al. [53] used a power law to describe the conversion of methane over graphite particles, and found a 4.4 reaction order and 208 kJ/mol activation energy. Their proposed model is valid for the 1260–1870 °C temperature range, maybe highlighting indirectly the limited reactivity of graphitic carbon [28]. Doubts appear that they might well be essentially describing the confounded effects of CMD and thermal decomposition.

Pinilla et al. [54] modeled the kinetics of CMD on activated carbon and carbon black in a TGA by monitoring the rate of carbon deposition. They observed an inflection point in the ratio of instantaneous to initial rates for a value of 90% of the initial amount of carbon deposited. After this inflection point, the rates increased and reached a maximum value, then decreased again. A summary of the kinetic characterization studies is presented in Table 1. We, however, note that to our surprise, while CMD catalysts have been extensively reviewed, the availability of kinetics expression is quite limited. Moreover, besides the development of detailed kinetics for SMR, we were unable to find kinetic mechanisms with their rates covering both the production of H_2 and the loss of activity of the catalyst due to deactivation by coke deposition.

Table 1. Overview of kinetics data available for the CMD using carbon-, iron-, and nickel-based catalysts.

Catalyst	Reaction Order 'n' with Respect to Methane	Pre-Exponential Factor (kmol kg_{cat}^{-1} $Pa^{-n}s^{-1}$)	Activation Energy (kJ mol^{-1})	Comments	References
Carbon-based					
Carbon black	0.5	-	141	TGA 800–950 °C	[54]
Activated carbon	0.5	-	238	TGA 800–950 °C	[54]
Activated carbon	2	4.28 $L^2g_{cat}^{-1}mol^{-1}s^{-1}$	163	Fixed bed 775–850 °C	[55]
Iron-based					
Fe	1	8.80×10^{-10}	54	TGA experiments, undisclosed composition 700–800 °C	[45]
Nickel-based					
Ni/SiO_2	1.4	2.24×10^{1}	61	Coprecipitation 550–650 °C	[46]
Ni-SBA-15	2	2.98×10^{3}	114	Electroless plating 525–600 °C	[47]
Ni/TiO_2	-	-	60	Wet impregnation 550–900 °C Kinetic model based on methane conversion	[56]

2.1.2. Iron-Based Catalysts

Fe-based catalysts operate at temperatures between 700 and 900 °C, and other metal catalysts such as Pd, Pt, Cr, Ru, Mo, and W have an even wider temperature window, ranging from 700 to 1000 °C [13,57,58]. Riley et al. [45] characterized the kinetics of methane pyrolysis over an iron-based catalyst of undisclosed composition using a first-order power law. They suggested that the catalytic decomposition of methane over an Fe-based catalyst starts with the chemisorption of methane, followed by the dehydrogenation of a CH_3–H bond (rate-limiting step). Density functional theory (DFT) calculations further refined the reaction mechanism analysis, and proposed the following mechanism [59]:

$$CH_4 \overset{Fe^0}{\longleftrightarrow} C_{amorphous} + 2H_2 \quad (2)$$

$$Fe^0 + C_{amorphous} \leftrightarrow Fe_3C \quad (3)$$

$$CH_4 \overset{Fe_3C/Fe^0}{\longleftrightarrow} C_{amorphous} + 2H_2 \quad (4)$$

$$C_{amorphous} \overset{Fe_3C}{\longleftrightarrow} C_{graphite} \quad (5)$$

2.1.3. Nickel-Based Catalysts

Metal-based catalysts are reported to produce carbon nanofibers and nanotubes that may have a higher value if the catalyst and the carbon product can be separated [37]. Ni-based catalysts usually show high catalytic activity and favor the production of carbon filaments or nanotubes at temperatures ranging from 500 to 700 °C. Zavarukhin & Kuvshinov [60] characterized the kinetics of CMD over Ni-based catalysts, proposing the

dissociative adsorption of methane followed by dehydrogenation, with both elementary steps acting as rate limiting on Ni-based catalysts (the group of Kuvshinov later mentioned that the dissociative adsorption was rate limiting for Ni catalysts with varying supports [61]). Snoeck et al. [44] identified the abstraction of the first H from the adsorbed CH_4* as the rate-limiting step on SMR catalysts.

Ashik et al. [46] characterized the catalytic decomposition of methane on a Ni/SiO_2 catalyst prepared by cum-modified Stöber co-precipitation using a 1.4-order power law. Taking advantage of the deactivation of Ni catalysts due to coke deposition, Zavarukhin & Kuvshinov [60] characterized the kinetics of nanofibrous carbon formation. They highlighted that the rate of formation increases until reaching a maximum value, then decreases, curiously enough due to the deactivation of the catalyst, along with a buildup of hydrogen. Chen & Lua [47] characterized the kinetics of a monometallic electroless plated Ni/SBA-15 catalyst using a power law combined to a time-dependent deactivation function. They proposed a second-order power law and explained the deactivation of the catalyst due to both the formation of filamentous carbons and coke covering the Ni particles.

The most complete coke deposition kinetic analysis on Ni was performed for SMR catalysts. Snoeck et al. [44] described the kinetics of coke formation leading to coke filaments using a set of nine elementary steps: four for the methane adsorption and dehydrogenation, one for the last dehydrogenation of CH* leading to coke, one for the H_2 release in the gas phase, and three elementary steps specifically describing the formation of coke filaments (dissolution, diffusion, and precipitation).

2.1.4. Deactivation Functions for the Characterization of Deactivation Due to Coking

As CMD leads to a continuous covering of the catalyst's active sites, a deactivation function describing the loss of activity with time on stream is required. The deactivation is often described by a power law, similarly to what is performed for the deactivation of the catalyst by sintering, e.g., using the generalized power law equation [62].

Chen and Lua [47] described with mixed success the deactivation of their Ni/SBA-15 catalyst, defining the activity as the ratio of the instantaneous rate of methane conversion to its initial value, using a 0.5 order and a 148 kJ mol^{-1}, in addition to a residence time dependency. Abbas & Daud [55] followed a similar approach (0.5 deactivation order, residence time dependency). Muradov et al. [63] correlated the loss of activity of activated carbon and carbon black with a decreased surface area, and used an empirical time-based decay function for activated carbon and carbon black.

2.1.5. Homogeneous Gas-Phase Methane Pyrolysis Kinetics

Obviously, in order to correctly simulate the CMD, the gas-phase homogeneous reactions should also be accounted for, especially if the high temperature at which methane pyrolysis occurs is aimed for. Interestingly, none of the detailed kinetic models (GRI-MECH 3.0, AramcoMech 2.0, etc.) are able to describe the pyrolysis of methane in the 730–2730 °C range, at least not at high pressures [64]. This is not a surprise as these models were developed for high-temperature processes in the presence of oxygen (combustion), and without considering the formation of polycyclic aromatic hydrocarbons, i.e., the precursors for solid carbon formation [65]. Recently, Shinde & Pradeep [66] implemented a detailed gas-phase kinetic model consisting of 37 species and 318 reactions in a chemical vapor deposition (CVD) reactor using an automatic mechanism generator and validated it against the experimental data in the 900–1100 °C, 10–100 kPa range. The model was subsequently reduced to 13 species and 29 reactions, and it agreed well with the detailed mechanism, especially at low inlet partial pressures of methane.

Younessi-Sinaki et al. [65] had previously studied the homogeneous decomposition of methane and ethane between 600 and 1600 °C by adapting the reaction mechanism of Appel et al. [67] based on the combustion of hydrocarbon fuels. Their model considered a well-stirred flow reactor at a constant temperature and pressure, involving 242 reactions and 75 species. Figure 3 shows the methane decomposition dependence on the temperature,

pressure, and residence time. The results obtained showed that the maximum H_2 yield at equilibrium was increasing when the pressure was decreasing. Moreover, at low pressures, very large residence times are required, corresponding to hydrogen amounts close to the equilibrium. However, when high pressures are employed, the peak of hydrogen production is reached very fast, with small residence times. When high temperatures are used (see curves around 1600 °C), combined with small residence times, the hydrogen produced reaches the equilibrium at all pressures. Figure 4 shows the decomposition of methane when various parameters such as the pressure, temperature, and residence time are changed in the presence of metal- and carbon-based catalysts. Interestingly, for carbon-based catalysts, higher temperatures are required compared to metal-based catalysts, i.e., homogeneous thermal decomposition should be accounted for.

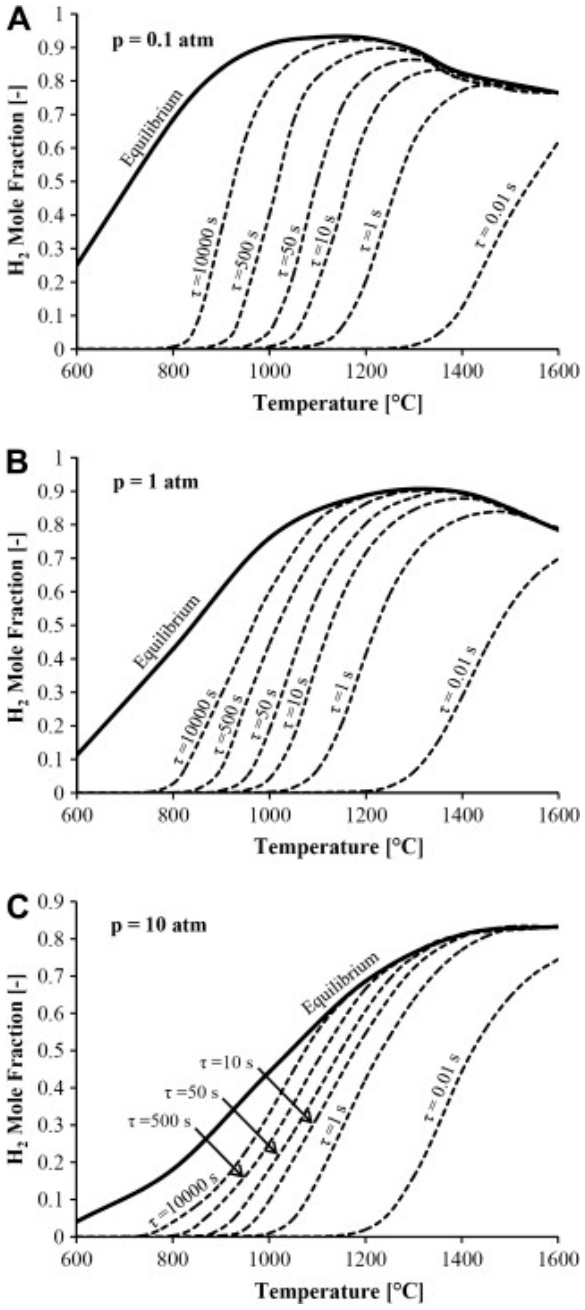

Figure 3. Mole fraction of hydrogen production from methane decomposition relative to temperature and residence time when pressure is 0.1 atm (**A**), 1 atm (**B**), and 10 atm (**C**), respectively. Reprinted with permission from Younessi-Sinaki et al. [65]. Copyright 2009 Elsevier.

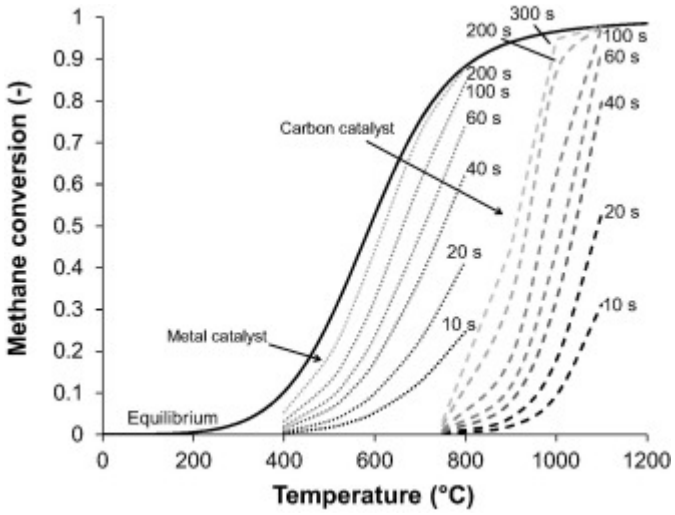

Figure 4. Methane decomposition dependence on temperature and residence time when metal (left set of curves) and carbon catalysts (right set of curves) are employed. Reprinted with permission from Keipi et al. [37]. Copyright 2016 Elsevier.

2.2. Reactor Technologies for Catalytic Methane Pyrolysis

We propose in this section to actualize the technology review around CMD by reviewing the patent literature. Doing so will complete the work of previous review articles on the topic (e.g., McConnachie et al. [68], mostly focusing on liquid metal catalysts, Schneider et al. [69], who only briefly summarized development on CMD due to the scope of their study, encompassing plasma and thermal methane pyrolysis).

The Hazer Group has disclosed a process for the production of hydrogen and graphitic carbon. The claims of their patents are over the use of iron oxides as catalysts, as well as the use of "one or various" reactors in series or in parallel operated in the 500–1200 °C range [70,71]. McConnachie et al. [68] further described the process as a series of three fluidized beds operated at decreasing pressure levels to optimize catalyst usage as they suffer from size reduction due to attrition. Their most recent patent describes the increased activity of their catalyst due to the effective removal of an "onion-like graphitic" layer on the catalyst due to attrition [71].

Innova Hydrogen Corp recently disclosed a membrane-based process for methane pyrolysis and for the separation of hydrogen and the produced graphene fibers [72]. The National Institute of Advanced Industrial Science And Technology (Japan) recently proposed a rotary kiln for the batchwise conversion of methane to hydrogen since catalyst deactivation with time on stream always occurs and can only be realistically reduced.

The Korean Institute of Industrial Technology proposed a sequential process where methane pyrolysis occurs, accumulating solid carbon in the bed, followed by CO formation via oxyfuel combustion. The heat from combustion is used for the sequential methane pyrolysis via heat storage in the pyrolysis reactor [73].

The preparation of a zinc–nickel organometallic framework, as well as single-atom nickel catalysts, was recently patented, where the inventor discloses a method to prevent the loss of dispersion of the active phase [74]. Unfortunately, no data on methane conversion or deactivation were provided in the description. Another interesting patent describes the use of waste materials (mill scale, steel, nickel and copper slags, with iron oxides) [75].

2.3. Electrified Reactor Technologies for Catalytic Methane Pyrolysis

While most of the reactors used at the lab scale are fixed beds, their use at an industrially relevant scale would make little sense, unless periodic operation with coke removal is considered acceptable. They are conventionally used for catalyst screening and kinetic characterization studies. For the deployment of this technology at industrially

relevant scales, continuous reactors for the solid phase are preferred to tackle the catalyst deactivation issue with time on stream. On top of that, care must be taken to replace conventional process heating (e.g., combustion of natural gas) if the CO_2 emissions are to be avoided. Electrification is one of the solutions, provided that low-carbon sources are used to generate the electricity. Power-to-heat, i.e., where electricity is used for heating at high temperatures, represents the first step for the chemical industry. The pace of the development of electrified technologies should be considerably increased: time is running short for the energy transition, and unfortunately, the most promising technologies for short-term electrification are still at the lab scale [76]. On top of that, if renewable electricity is to be used to increase sustainability, reactor control strategies are required to adapt the operation of electrified reactors to the varying nature of sustainable electricity, while producing consistent products.

As an example of the benefits of electrifying reactor technologies, 25% of the CO_2 emissions from steam methane reforming (SMR) can be tackled via electrification (from fuel combustion). Power-to-heat can indeed reduce the scope 2 emissions, while scope 3 emission reductions involve a drastic redesign of SMR units. In addition, electrification has the power to shift the SMR reactor design from its current heat transfer limitation to that of a kinetic regime [77], thus involving a better usage of catalysts. Devising innovative electrified units, while at the same time extracting the scaling rules for their fast commercial deployment, is crucial for the chemical industry.

The question that arises then is which electrification techniques should be prioritized, especially for the short-term urgent minimization of the CO_2 emissions associated with the H_2 production? Stankiewicz & Nigar [78] concluded that the electrification techniques aiming at modifying the reaction mechanisms were complex to design and scale-up (electrocatalytic and sonochemical reactors), inefficient (photocatalytic), or they suffered from high energy requirements, low selectivity and conversion, and challenging scale-up (plasma). With respect to power-to-heat, microwave-based technologies suffer challenging radiation supply and low efficiencies (limited penetration depth and low efficiency in converting electrical energy into thermal energy, i.e., in the 50–60% range [79]). In the specific case of gas–solid chemistries, achieving a uniform catalyst temperature is still an unresolved issue. They identified ohmic heating and inducting heating as the most promising, with ohmic heating mostly applicable for gas–solid applications, while induction heating was applicable to any multiphase reacting flows. We respectfully disagree with their views as ohmic heating is widely used in the food industry and for organic synthesis, i.e., for liquid-phase reacting flows [79].

With respect to electrical heating, ExxonMobil recently proposed a stacked fluidized bed concept with electrical heating in the initial stage in a H_2-rich atmosphere gas to minimize the formation of coke [80]. Their concept allows for avoiding the CO_2 emissions due to conventional process heating. The patent does not, however, clarify what techniques are used in particular for "electrical heating". BASF is also active in the electrification of the methane pyrolysis process, where here too, little information is available regarding the electrical techniques envisioned for this purpose [81,82], even though some published information points to the use of induction heating [83,84].

Total Energies SE recently described the use of an electrothermal fluidized bed [85–87] for the steam reforming of hydrocarbons [88], as well as for the direct pyrolysis of methane to produce solid carbon, H_2, and C2+ [89]. An electrothermal fluidized bed is obtained when flowing an electrical current in a fluidized bed of electrically conducting particles: the electrical energy is converted into heat via the Joule effect due to the particles' resistivity. To do so, two electrodes are immersed in the bed. The most common configuration involves center graphite electrodes surrounded by a coaxial second electrode [85,90,91] (Figure 5). The parallel electrode configuration for catalytic reaction has been less discussed [92]. Shockwave heating occurs via two mechanisms: (i) short duration particle-to-particle collisions (instantaneous electrical contact) and (ii) short-lived micro-plasma arcs percolating throughout the bed at short interparticle distances. The net result is alternating ohmic

heating due to both mechanisms. Current flows when the concentration of conductive particles reaches a critical concentration, and the highest temperature is obtained where the interelectrode distance is minimal.

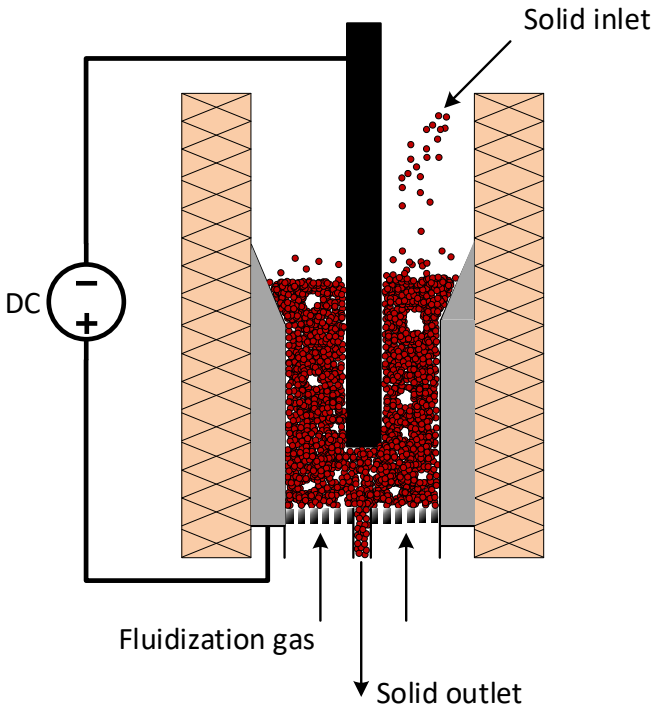

Figure 5. Schematic view of an electrothermal fluidized bed with the coaxial electrode configuration used for continuous solid processing. In order to dissipate heat via the Joule effect, the solid bed particles are electrically conductive. Adapted from [85].

The electrification of a fluidized bed is more than a mere heating mechanism: it affects the hydrodynamics of the bed. The complex interplay between hydrodynamics and electrical effects were recognized in the 1970s: strings of particles appear in the direction of the average electric field, resulting in elongated bubbles, affecting particle motion in the vicinity of the bubbles, decreased particle mixing in general, increased channeling risks, and minimum fluidization velocity [93]. The presence of the electrodes naturally perturbs the bed: the packed bed regime gradually switches to a sub-standard bubbling mode, where the fluidization state is only achieved in the close vicinity of the immersed electrode(s). Interestingly, increasing the gas flowrate does not suffice to shift from this weak fluidization state to a fully bubbling regime: the control of the specific electrical resistance (SER) is the key parameter, which depends on both the solid bed (material, particle size, bed height, and expansion), physical parameters (current density, in turn affected by the positioning of the electrodes), fluidization gas and gaseous products formed, reactor size (diameter), as well as fluidization regime (also affected by the configuration of the electrodes) [85].

Also relying on shockwave heating, Dong et al. [94] demonstrated the use of a "programmable heating and quenching" (PHQ) system for methane pyrolysis, yielding a C_2 selectivity of approximately 80%. The PHQ switches from 650 to 2000 K in milliseconds, thus favoring the methane-coupling route versus the formation of coke, using a porous carbon paper as the heating element.

Microwave heating of carbon particles has also been described for methane pyrolysis [95], leading to semi-graphitic pyrolytic carbon products that could be used as anode material in Na-ion batteries [96]. Interestingly, Hamzehlouia and Chaouki [97] described a method for the coating of particles in a microwave-heated fluidized bed, opening the door for the use of any type of catalyst for the microwave-assisted methane pyrolysis. An intriguing emerging concept is the use of pressure waves for chemical conversion, e.g.,

Rudolph & Atakan [98] recently proposed a motored piston engine to convert mechanical to chemical energy for the pyrolysis of methane. The main pyrolysis products are acetylene, ethylene, and benzene. As with the PHQ concept of Dong et al. [94], the reaction is not selective for carbonaceous solid products, but since benzene is formed, we can expect that we are not too far from soot precursors and coke formation. A pulsed compression reactor (PCR) able to reach 600 bar in a single pulse was also recently described for that purpose [64].

3. Solid Carbon Deposition and Gasification

In order to assess whether the combined process of CMD coupled with coke gasification from the CO_2 present in biogas, enhanced by steam, is feasible, and to identify the optimal catalytic system and operating conditions, we review in this section the available studies on coke deposition and its kinetics, as well as the kinetics of catalytic coke gasification.

3.1. Coke Deposition

Keipi et al. [37] provided an overview of the types of carbon resulting from methane pyrolysis. The authors have shown that the morphology of the obtained solid carbon is a function of the reaction conditions, including the presence and type of the catalyst employed. Figure 6 shows the various types of carbon produced during methane pyrolysis relative to the reaction temperature and type of catalyst. Interestingly, carbon black (although carbonaceous materials obtained as an undesired byproduct are usually expressed as "black carbon", the term "carbon black" is used here based on the observation of Guil-Lopez et al. [99] that the produced carbon has a similar structure to carbon black) and graphite-like carbon are predominantly produced when a purely thermal process is considered and when carbon-based catalysts are employed. On top of this, the limited understanding of the behavior of activated carbon at the molecular level arises from the fact that its atomic structure is unknown [100]. Recent studies on the deposition of carbon from methane pyrolysis on various porous materials (e.g., C, SiC, α, and γ-Al_2O_3) have shown that porous media exhibit a maximum achievable loading, and that this is not a result of pore blockage [101]. The authors noticed that smaller pores are not filled to the same extent as larger pores, and they speculated that the smaller pores prevent the carbonaceous intermediate from forming into the pore. The larger pores are indicated to be prone to a similar deactivation mechanism comparable to nonporous α-Al_2O_3 particles, described by the same authors [49].

On the other hand, metal catalysts, such as Co-, Fe-, or Ni-based, are more prone to favor the production of filamentous-type carbon, such as nanofibers, nanotubes, and carbon plates, among others. Carbon-based catalysts may offer various advantages compared with metal-loaded catalysts [102–104]. For instance, the lower cost of carbon materials, combined with the ability to tolerate aggressive chemicals and high temperatures, and the potential for better marketability of the carbon product, make them desirable characteristics for the industry. An important advantage is that the catalyst may not need to be separated from the product [13]. Different types of carbon materials, such as activated and carbon black, microcrystalline graphites, and nanostructured carbons, have been investigated as catalysts for methane pyrolysis [28,105]. Experimental observations showed that the catalytic activity in the methane decomposition reaction increases with the carbon surface area [51], in fact, with the surface concentration of defects, vacancies, and low-coordination sites [106]. The decrease in the catalytic activity with the loss in the carbon surface area would be due to the deposition of catalytically inactive carbon species produced from methane. This indicates that the carbon catalyst employed must have a certain concentration of defects in the carbon surface and should be maintained and/or regenerated during the reaction.

Vohler et al. [19] studied the deposition of pyrolytic carbon in the pore system of graphite. The authors were able to show from both theoretical and experimental work that the deposition of carbon occurs preferentially inside the pores when the rate of deposition is

lower. To achieve the required control over the rate of deposition, the reaction temperature and gas temperature can be selected as low as possible.

Kreuger et al. [101] characterized the coke deposition kinetics on porous α- and γ-Al_2O_3, SiC, and C carriers using the product of a first-order reaction with respect to methane, and a dampening factor describing the fraction of pores occupied with carbon. They relied on this dampening factor (yielding a null value at high coking rates) to simulate the observed stopping in carbon deposition, even when the internal area is still available. They did not propose numerical values of the pre-exponential factor and activation energy due to the limited temperature range at which their measurements were made.

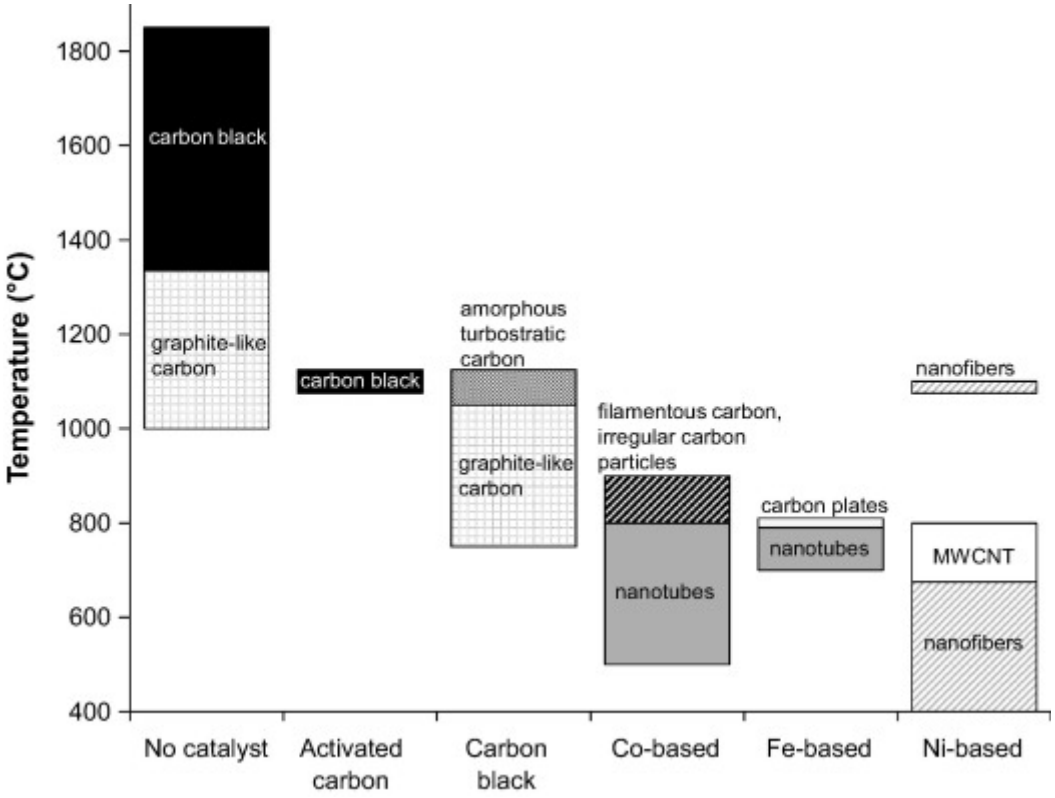

Figure 6. Carbon product windows obtained during methane pyrolysis relative to the process temperature for catalytic and noncatalytic systems. Reprinted with permission from Keipi et al. [37]. Copyright 2016 Elsevier.

3.2. Gasification Kinetics

Early studies performed by Ergun [18] on the reaction kinetics of the CO_2 gasification of coke deposited on charcoal and activated graphite, as well as nonporous Ceylon graphite, revealed that the reaction rate is proportional to the concentration of carbon-occupied sites, underlying dynamic two-phase gas–solid oxygen-exchange reactions: an oxygen atom is extracted from the CO_2 molecule, producing CO and creating an occupied site. At the same time, CO is thought to remove the oxygen from the occupied site, reversibly forming CO_2. It was suggested that the carbon transfer from the solid phase to the gas phase coming from the occupied sites was the rate-determining step. For the nonporous Ceylon graphite, the number of reaction sites increased with the decrease in the particle size, in contrast with what was observed for porous carbon. As the same values of the equilibrium constant and rate constant were assumed to apply to all types of carbon, the number of reaction sites per weight of carbon was the only property affecting the rate, leading to the conclusion that the concentration of reaction sites constitutes the direct measure of reactivity. The equilibrium has a noticeable effect on the gasification rate of gasification. For instance, if the ratio of carbon monoxide to CO_2 is maintained at 1 in the gas phase when the reaction temperature is raised from 700 to 1000 °C, the number of occupied sites would increase by

a factor of 16, and when raised to 1400 °C, by a factor of 38. Similarly, if the ratio of carbon monoxide to CO_2 is maintained at 0.1, the corresponding increase would be by factors of 22 and 140. This points to the fact that CO retards the rate by reducing the concentration of occupied sites.

In a recent study, Kreuger et al. [17] investigated the gasification of carbon produced during methane pyrolysis on nonporous a-Al_2O_3, and how to predict its gasification rates with steam, CO_2, and air between 950 and 1150 °C. They observed that neither a conventional first-order model nor carbon characteristics are suitable pathways for describing the measured gasification rates. The authors included the pyrolysis parameters to construct a gasification model. They compiled various observations from the gasification measurements. For instance, Figure 7 shows the gasification rates measured in a single-particle reactor as a function of the pyrolysis time. When steam and CO_2 are used as gasification gases, it was noted that the gasification rate is initially characterized by high values for the carbon deposits produced at a low pyrolysis time (defined as the time the particle is in contact with CH_4 at the pyrolysis temperature).

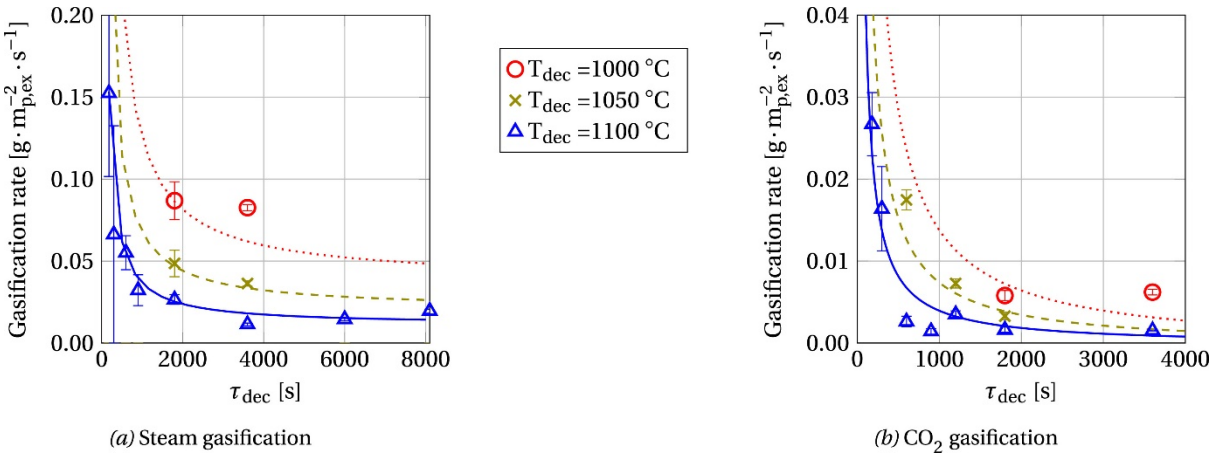

(a) Steam gasification *(b)* CO_2 gasification

Figure 7. Gasification rates measured in a single-particle reactor as a function of pyrolysis time for (**a**) steam and (**b**) CO_2 gasification, respectively. Lines represent the gasification model predictions. Reprinted from Kreuger et al. [17]. Copyright 2022 Elsevier.

When the pyrolysis time is increased, the gasification rate is found to decrease rapidly and, ultimately, approaches a constant value. Similarly, when the pyrolysis temperature is increased, the gasification rate was found to decrease. The reactivity for CO_2 was found to be much lower than for steam under the conditions investigated by the authors. It was suggested that some characteristics of the carbon must influence the gasification rate, and changes in the carbon reactivity occur when methane is present in some fraction of the atmosphere.

Regeneration studies on the spent carbon-based catalyst (e.g., activated carbon), performed by Yang et al. [107], interestingly showed that deep regeneration based on H_2O and O_2 used together was suitable for resuming catalyst activity, and it was superior to H_2O, O_2, and CO_2 applied individually. The gasification of the formed carbonaceous deposit with CO_2, either in pulses or in parallel as a mixture with methane, was studied by Adamska et al. [108]. The authors reported a reduction in catalyst deactivation and an increase in the H_2 content of the product due to the introduction of CO_2 into the reaction system. It was suggested that when CO_2 is introduced into the reactor simultaneously with methane, the rates of mainly three processes are affected: carbon deposition, gasification of the carbon deposit, and partial gasification of the carbon catalysts. When methane decomposition cycles were alternated with gasification steps using CO_2 at 900 °C, 950 °C, and 1000 °C, the results showed a strong temperature dependence of the gasification process [109]. Moreover, it was observed that the gasification reactivity changed with the methane conversion, and maximum values for both the virgin and deactivated carbon catalysts were observed

at the decomposition temperature of 950 °C. The reactivity of the gasification was seen to decrease after only three cycles at 1000 °C. When the temperature was decreased to 950 °C or 900 °C, no significant change was reported. The same authors showed that the initial activity and the ultimate mass gain of the catalyst decreased after each regeneration cycle at both reaction temperatures of 850 °C and 950 °C [110]. When the reaction was performed at 950 °C, a steep decrease was observed between the first and the sixth reaction cycles, for both the initial activity and the ultimate mass gain, when the CO_2 gasification temperature was increased from 900 °C to 1000 °C.

On the specific topic of the gasification of pyrolytic coke deposited during methane cracking, Pinilla et al. [27] studied the regeneration of a carbon-based catalyst using CO_2. They purposely coked activated carbon at 850 °C for 8 h in CMD conditions and studied their regeneration between 700 and 950 °C in a fluidized bed. In this case, the gasification rates were negligible below 900 °C. At 900 °C, they were able to recover 100% of the BET surface, and 70% of the surface oxygenated groups, essential for the reactivation of the catalysts. After 3 h of coking (850 °C)/regeneration (900 °C) cycles, the CMD activity dropped to less than 5% of the initial activity. However, for regeneration cycles at 950 °C for 2 h, the activity of the activated carbon was almost completely recovered, at the expense of a continuous decrease in the textural properties. Dufour et al. [111] showed that the activity of wood char could be recovered via steam gasification, and even exceed the activity of fresh char for CMD.

4. Conclusions

In this review, we aim to summarize the key particularities of methane pyrolysis when potentially combined with the gasification of the produced pyrolytic carbon. Although the current state-of-the-art does not provide sufficient information for considering the synchronization of methane pyrolysis and carbon gasification, the current urgency for CO_2-free H_2 technologies makes this approach a promising technological solution. By using active and selective catalysts combined with thermal energy supplied from renewable sources, this method might provide a transition to cleaner energy solutions and allow time for more green technologies to mature technologically and in their processes. The difficulty also lies in the fact that the term "coke deposit" is used in some instances as a general description for the carbonaceous material resulting from the process but lacking proper characterization. This makes the correlation between reaction parameters and potential gasification conditions a difficult task. There is a clear need for detailed kinetics.

Coupling methane pyrolysis with the gasification of carbon might offer an ideal solution for an efficient and environmentally responsible production of H_2, enabling carbon-free technology and a viable solution for the produced carbon byproduct. It is important to mention that this process does not require a market for the carbonaceous material, making the technology independent of market fluctuations and third-party financial interests, thereby increasing economic transparency and stability.

Our emphasis was on the kinetics of methane pyrolysis, carbon deposition, and carbon gasification as these are among the most critical aspects in the process design. Moreover, a thorough understanding of the type of pyrolytic carbon linked with the pyrolysis conditions and its potential variations is necessary for stable and predictable reactivity. Indeed, differences between the reactivities of crystalline vs. amorphous carbon might pose various challenges. Generally speaking, crystalline materials offer well-defined energy points, making gasification more achievable. On the other hand, amorphous materials are more energetically challenging, and their reactivity in selective reactions might present difficulties. Finding the proper window for the kinetics of the various reactions so that the conditions are suitable for both methane cracking and carbon gasification is one of the main challenges. As stated by Pinilla et al. [27], a better understanding of the deposed carbon should guide our choice for optimal regeneration conditions.

The future research should focus on aiming at a better understanding of the carbonaceous products formed as a function of the operating conditions, linked to a thorough

investigation of catalyst regeneration. In addition, for proper reactor technology design and optimization, detailed kinetics of CMD should be taken into consideration and the catalyst deactivation due to carbon formation should be determined. The deactivation functions should be elaborated based on the catalyst state, and not as a function of time on stream. It is only with these data at hand that we will be able to validate the technical feasibility of our proposed process for the combined CMD and coke gasification using the CO_2 present in the biogas. It is interesting to note that by doing so, we will contribute to the very industrially important field of the development of coke-resisting catalysts.

Author Contributions: Conceptualization, P.P.; methodology, P.P.; writing—original draft preparation, P.P.; writing—review and editing, C.-R.B., I.P.S., H.D.Y. and N.B.K.; visualization, P.P.; supervision, P.P.; project administration, P.P. All authors have read and agreed to the published version of the manuscript.

Funding: This research received no external funding.

Conflicts of Interest: The authors declare no conflict of interest.

References

1. Agency, I.E. *The Future of Hydrogen*; OECD: Paris, France, 2019.
2. Van Geem, K.M.; Galvita, V.V.; Marin, G.B. Making chemicals with electricity. *Science* **2019**, *364*, 734–735. [CrossRef] [PubMed]
3. Erisman, J.W.; Sutton, M.A.; Galloway, J.; Klimont, Z.; Winiwarter, W. How a century of ammonia synthesis changed the world. *Nat. Geosci.* **2008**, *1*, 636–639. [CrossRef]
4. Air Liquide Paves the Way for Ammonia Conversion into Hydrogen with New Cracking Technology. Available online: https://www.airliquide.com/group/press-releases-news/2023-03-23/air-liquide-paves-way-ammonia-conversion-hydrogen-new-cracking-technology (accessed on 8 August 2023).
5. IEA. *Hydrogen Patents for a Clean Energy Future*; IEA: Paris, France, 2023.
6. Lubbe, F.; Rongé, J.; Bosserez, T.; Martens, J.A. Golden hydrogen. *Curr. Opin. Green Sustain. Chem.* **2023**, *39*, 100732. [CrossRef]
7. Between Green and Blue: A debate on Turquoise Hydrogen. Available online: https://fsr.eui.eu/between-green-and-blue-a-debate-on-turquoise-hydrogen/ (accessed on 1 September 2023).
8. Verbeeck, K.; Buelens, L.C.; Galvita, V.V.; Marin, G.B.; Van Geem, K.M.; Rabaey, K. Upgrading the value of anaerobic digestion via chemical production from grid injected biomethane. *Energy Environ. Sci.* **2018**, *11*, 1788–1802. [CrossRef]
9. Ryckebosch, E.; Drouillon, M.; Vervaeren, H. Techniques for transformation of biogas to biomethane. *Biomass Bioenergy* **2011**, *35*, 1633–1645. [CrossRef]
10. Abánades, A.; Rathnam, R.K.; Geißler, T.; Heinzel, A.; Mehravaran, K.; Müller, G.; Plevan, M.; Rubbia, C.; Salmieri, D.; Stoppel, L.; et al. Development of methane decarbonisation based on liquid metal technology for CO_2-free production of hydrogen. *Int. J. Hydrogen Energy* **2016**, *41*, 8159–8167. [CrossRef]
11. Sánchez-Bastardo, N.; Schlögl, R.; Ruland, H. Methane Pyrolysis for CO_2-Free H_2 Production: A Green Process to Overcome Renewable Energies Unsteadiness. *Chem. Ing. Tech.* **2020**, *92*, 1596–1609. [CrossRef]
12. Zhang, J.; Li, X.; Chen, H.; Qi, M.; Zhang, G.; Hu, H.; Ma, X. Hydrogen production by catalytic methane decomposition: Carbon materials as catalysts or catalyst supports. *Int. J. Hydrogen Energy* **2017**, *42*, 19755–19775. [CrossRef]
13. Muradov, N.Z.; Veziroğlu, T.N. From hydrocarbon to hydrogen–carbon to hydrogen economy. *Int. J. Hydrogen Energy* **2005**, *30*, 225–237. [CrossRef]
14. Jorschick, H.; Bösmann, A.; Preuster, P.; Wasserscheid, P. Charging a Liquid Organic Hydrogen Carrier System with H_2/CO_2 Gas Mixtures. *ChemCatChem* **2018**, *10*, 4329–4337. [CrossRef]
15. Jorschick, H.; Vogl, M.; Preuster, P.; Bösmann, A.; Wasserscheid, P. Hydrogenation of liquid organic hydrogen carrier systems using multicomponent gas mixtures. *Int. J. Hydrogen Energy* **2019**, *44*, 31172–31182. [CrossRef]
16. Reuß, M.; Grube, T.; Robinius, M.; Preuster, P.; Wasserscheid, P.; Stolten, D. Seasonal storage and alternative carriers: A flexible hydrogen supply chain model. *Appl. Energy* **2017**, *200*, 290–302. [CrossRef]
17. Kreuger, T.; Bos, A.N.R.; Kersten, S.R.A. Predicting gasification rates of pyrolytic graphite deposited from methane. *Chem. Eng. J.* **2022**, *440*, 135487. [CrossRef]
18. Ergun, S. Kinetics of the Reaction of Carbon with Carbon Dioxide. *J. Phys. Chem.* **1956**, *60*, 480–485. [CrossRef]
19. Vohler, O.; Reiser, P.L.; Sperk, E. Deposition of pyrolytic carbon in the pores of graphite bodies—I. Introduction to and results of deposition experiments using methane. *Carbon* **1968**, *6*, 397–403. [CrossRef]
20. Lobo, L.S.; Carabineiro, S.A.C. Kinetics and mechanism of catalytic carbon gasification. *Fuel* **2016**, *183*, 457–469. [CrossRef]
21. Zhang, Y.; Hara, S.; Kajitani, S.; Ashizawa, M. Modeling of catalytic gasification kinetics of coal char and carbon. *Fuel* **2010**, *89*, 152–157. [CrossRef]
22. Lobo, L.S. Intrinsic kinetics in carbon gasification: Understanding linearity, "nanoworms" and alloy catalysts. *Appl. Catal. B: Environ.* **2014**, *148–149*, 136–143. [CrossRef]

23. Lobo, L.S.; Carabineiro, S.A.C. Catalytic carbon gasification: Understanding catalyst-carbon contact and rate jump behavior with air. *Fuel Process. Technol.* **2018**, *179*, 313–318. [CrossRef]
24. Arnold, R.A.; Motta, I.L.; Hill, J.M. Impact of particle size and catalyst dispersion on gasification rates measured in a thermogravimetric analysis unit: Case study of carbon black catalyzed by potassium or calcium. *Fuel* **2021**, *288*, 119677. [CrossRef]
25. Xu, B.; Cao, Q.; Kuang, D.; Gasem, K.A.M.; Adidharma, H.; Ding, D.; Fan, M. Kinetics and mechanism of CO_2 gasification of coal catalyzed by Na_2CO_3, $FeCO_3$ and Na_2CO_3–$FeCO_3$. *J. Energy Inst.* **2020**, *93*, 922–933. [CrossRef]
26. Dahou, T.; Defoort, F.; Khiari, B.; Labaki, M.; Dupont, C.; Jeguirim, M. Role of inorganics on the biomass char gasification reactivity: A review involving reaction mechanisms and kinetics models. *Renew. Sustain. Energy Rev.* **2021**, *135*, 110136. [CrossRef]
27. Pinilla, J.L.; Suelves, I.; Utrilla, R.; Gálvez, M.E.; Lázaro, M.J.; Moliner, R. Hydrogen production by thermo-catalytic decomposition of methane: Regeneration of active carbons using CO_2. *J. Power Sources* **2007**, *169*, 103–109. [CrossRef]
28. Muradov, N. Catalysis of methane decomposition over elemental carbon. *Catal. Commun.* **2001**, *2*, 89–94. [CrossRef]
29. Bajec, D.; Kostyniuk, A.; Pohar, A.; Likozar, B. Micro-kinetics of non-oxidative methane coupling to ethylene over Pt/CeO_2 catalyst. *Chem. Eng. J.* **2020**, *396*, 125182. [CrossRef]
30. Nishikawa, Y.; Ogihara, H.; Yamanaka, I. Liquid-Metal Indium Catalysis for Direct Dehydrogenative Conversion of Methane to Higher Hydrocarbons. *ChemistrySelect* **2017**, *2*, 4572–4576. [CrossRef]
31. Sheng, H.; Schreiner, E.P.; Zheng, W.; Lobo, R.F. Non-oxidative Coupling of Methane to Ethylene Using Mo2C/[B]ZSM-5. *ChemPhysChem* **2018**, *19*, 504–511. [CrossRef] [PubMed]
32. Gerceker, D.; Motagamwala, A.H.; Rivera-Dones, K.R.; Miller, J.B.; Huber, G.W.; Mavrikakis, M.; Dumesic, J.A. Methane Conversion to Ethylene and Aromatics on PtSn Catalysts. *ACS Catal.* **2017**, *7*, 2088–2100. [CrossRef]
33. Guo, X.G.; Fang, G.Z.; Li, G.; Ma, H.; Fan, H.J.; Yu, L.; Ma, C.; Wu, X.; Deng, D.H.; Wei, M.M.; et al. Direct, Nonoxidative Conversion of Methane to Ethylene, Aromatics, and Hydrogen. *Science* **2014**, *344*, 616–619. [CrossRef]
34. Ji, Y.; Palmer, C.; Foley, E.E.; Giovine, R.; Yoshida, E.; Sebti, E.; Patterson, A.R.; McFarland, E.; Clément, R.J. Valorizing the carbon byproduct of methane pyrolysis in batteries. *Carbon* **2023**, *204*, 26–35. [CrossRef]
35. Chesnokov, V.V.; Chichkan, A.S. Production of hydrogen by methane catalytic decomposition over Ni–Cu–Fe/Al_2O_3 catalyst. *Int. J. Hydrogen Energy* **2009**, *34*, 2979–2985. [CrossRef]
36. Guéret, C.; Daroux, M.; Billaud, F. Methane pyrolysis: Thermodynamics. *Chem. Eng. Sci.* **1997**, *52*, 815–827. [CrossRef]
37. Keipi, T.; Tolvanen, K.E.S.; Tolvanen, H.; Konttinen, J. Thermo-catalytic decomposition of methane: The effect of reaction parameters on process design and the utilization possibilities of the produced carbon. *Energy Convers. Manag.* **2016**, *126*, 923–934. [CrossRef]
38. Parkinson, B.; Patzschke, C.F.; Nikolis, D.; Raman, S.; Dankworth, D.C.; Hellgardt, K. Methane pyrolysis in monovalent alkali halide salts: Kinetics and pyrolytic carbon properties. *Int. J. Hydrogen Energy* **2021**, *46*, 6225–6238. [CrossRef]
39. Bae, D.; Kim, Y.; Ko, E.H.; Ju Han, S.; Lee, J.W.; Kim, M.; Kang, D. Methane pyrolysis and carbon formation mechanisms in molten manganese chloride mixtures. *Appl. Energy* **2023**, *336*, 120810. [CrossRef]
40. Dors, M.; Nowakowska, H.; Jasiński, M.; Mizeraczyk, J. Chemical Kinetics of Methane Pyrolysis in Microwave Plasma at Atmospheric Pressure. *Plasma Chem. Plasma Process.* **2014**, *34*, 313–326. [CrossRef]
41. Baranov, I.E.; Demkin, S.A.; Zhivotov, V.K.; Nikolaev, I.I.; Rusanov, V.D.; Fedotov, N.G. Methane Pyrolysis Stimulated by Admixture of Atomic Hydrogen: 2. Mechanism Analysis and Kinetics Calculation. *High Energy Chem.* **2005**, *39*, 268–272. [CrossRef]
42. Mao, X.; Chen, Q.; Guo, C. Methane pyrolysis with N_2/Ar/He diluents in a repetitively-pulsed nanosecond discharge: Kinetics development for plasma assisted combustion and fuel reforming. *Energy Convers. Manag.* **2019**, *200*, 112018. [CrossRef]
43. Alstrup, I.; Teresa Tavares, M. The kinetics of carbon formation from CH_4 + H_2 on a silica-supported nickel catalyst. *J. Catal.* **1992**, *135*, 147–155. [CrossRef]
44. Snoeck, J.W.; Froment, G.F.; Fowles, M. Kinetic Study of the Carbon Filament Formation by Methane Cracking on a Nickel Catalyst. *J. Catal.* **1997**, *169*, 250–262. [CrossRef]
45. Riley, J.; Atallah, C.; Siriwardane, R.; Stevens, R. Technoeconomic analysis for hydrogen and carbon Co-Production via catalytic pyrolysis of methane. *Int. J. Hydrogen Energy* **2021**, *46*, 20338–20358. [CrossRef]
46. Ashik, U.P.M.; Wan Daud, W.M.A.; Abbas, H.F. Methane decomposition kinetics and reaction rate over Ni/SiO_2 nanocatalyst produced through co-precipitation cum modified Stöber method. *Int. J. Hydrogen Energy* **2017**, *42*, 938–952. [CrossRef]
47. Chen, Q.; Lua, A.C. Kinetic reaction and deactivation studies on thermocatalytic decomposition of methane by electroless nickel plating catalyst. *Chem. Eng. J.* **2020**, *389*, 124366. [CrossRef]
48. Wang, H.Y.; Lua, A.C. Deactivation and kinetic studies of unsupported Ni and Ni–Co–Cu alloy catalysts used for hydrogen production by methane decomposition. *Chem. Eng. J.* **2014**, *243*, 79–91. [CrossRef]
49. Kreuger, T.; van Swaaij, W.P.M.; Bos, A.N.R.; Kersten, S.R.A. Methane decomposition kinetics on unfunctionalized alumina surfaces. *Chem. Eng. J.* **2022**, *427*, 130412. [CrossRef]
50. Xavier, N.F., Jr.; Bauerfeldt, G.F.; Sacchi, M. First-Principles Microkinetic Modeling Unravelling the Performance of Edge-Decorated Nanocarbons for Hydrogen Production from Methane. *ACS Appl. Mater. Interfaces* **2023**, *15*, 6951–6962. [CrossRef] [PubMed]
51. Muradov, N. Thermocatalytic CO_2-free production of hydrogen from hydrocarbon fuels. In Proceedings of the 2000 Hydrogen Program Review, San Ramon, CA, USA, 5 September–5 November 2000.

52. Trommer, D.; Hirsch, D.; Steinfeld, A. Kinetic investigation of the thermal decomposition of CH_4 by direct irradiation of a vortex-flow laden with carbon particles. *Int. J. Hydrogen Energy* **2004**, *29*, 627–633. [CrossRef]
53. Dahl, J.K.; Barocas, V.H.; Clough, D.E.; Weimer, A.W. Intrinsic kinetics for rapid decomposition of methane in an aerosol flow reactor. *Int. J. Hydrogen Energy* **2002**, *27*, 377–386. [CrossRef]
54. Pinilla, J.L.; Suelves, I.; Lázaro, M.J.; Moliner, R. Kinetic study of the thermal decomposition of methane using carbonaceous catalysts. *Chem. Eng. J.* **2008**, *138*, 301–306. [CrossRef]
55. Abbas, H.F.; Daud, W.M.A.W. Hydrogen production by thermocatalytic decomposition of methane using a fixed bed activated carbon in a pilot scale unit: Apparent kinetic, deactivation and diffusional limitation studies. *Int. J. Hydrogen Energy* **2010**, *35*, 12268–12276. [CrossRef]
56. Sharif Zein, S.H.; Mohamed, A.R.; Talpa Sai, P.S. Kinetic Studies on Catalytic Decomposition of Methane to Hydrogen and Carbon over Ni/TiO_2 Catalyst. *Ind. Eng. Chem. Res.* **2004**, *43*, 4864–4870. [CrossRef]
57. Shah, N.; Panjala, D.; Huffman, G.P. Hydrogen Production by Catalytic Decomposition of Methane. *Energy Fuels* **2001**, *15*, 1528–1534. [CrossRef]
58. Aiello, R.; Fiscus, J.E.; zur Loye, H.-C.; Amiridis, M.D. Hydrogen production via the direct cracking of methane over Ni/SiO_2: Catalyst deactivation and regeneration. *Appl. Catal. A: Gen.* **2000**, *192*, 227–234. [CrossRef]
59. Zhou, L.; Enakonda, L.R.; Harb, M.; Saih, Y.; Aguilar-Tapia, A.; Ould-Chikh, S.; Hazemann, J.-L.; Li, J.; Wei, N.; Gary, D.; et al. Fe catalysts for methane decomposition to produce hydrogen and carbon nano materials. *Appl. Catal. B Environ.* **2017**, *208*, 44–59. [CrossRef]
60. Zavarukhin, S.G.; Kuvshinov, G.G. The kinetic model of formation of nanofibrous carbon from CH_4–H_2 mixture over a high-loaded nickel catalyst with consideration for the catalyst deactivation. *Appl. Catal. A Gen.* **2004**, *272*, 219–227. [CrossRef]
61. Ermakova, M.A.; Ermakov, D.Y.; Kuvshinov, G.G. Effective catalysts for direct cracking of methane to produce hydrogen and filamentous carbon: Part I. Nickel catalysts. *Appl. Catal. A: Gen.* **2000**, *201*, 61–70. [CrossRef]
62. Bartholomew, C.H. Mechanisms of catalyst deactivation. *Appl. Catal. A: Gen.* **2001**, *212*, 17–60. [CrossRef]
63. Muradov, N.; Smith, F.; T-Raissi, A. Catalytic activity of carbons for methane decomposition reaction. *Catal. Today* **2005**, *102-103*, 225–233. [CrossRef]
64. Slotboom, Y.; Kersten, S.R.A. Mapping of operating windows for methane and ethane pyrolysis in the pulsed compression reactor by experiments and modelling. *Chem. Eng. J.* **2023**, *468*, 143522. [CrossRef]
65. Younessi-Sinaki, M.; Matida, E.A.; Hamdullahpur, F. Kinetic model of homogeneous thermal decomposition of methane and ethane. *Int. J. Hydrogen Energy* **2009**, *34*, 3710–3716. [CrossRef]
66. Shinde, V.M.; Pradeep, P. Detailed gas-phase kinetics and reduced reaction mechanism for methane pyrolysis involved in CVD/CVI processes. *J. Anal. Appl. Pyrolysis* **2021**, *154*, 104998. [CrossRef]
67. Appel, J.; Bockhorn, H.; Frenklach, M. Kinetic modeling of soot formation with detailed chemistry and physics: Laminar premixed flames of C2 hydrocarbons. *Combust. Flame* **2000**, *121*, 122–136. [CrossRef]
68. McConnachie, M.; Konarova, M.; Smart, S. Literature review of the catalytic pyrolysis of methane for hydrogen and carbon production. *Int. J. Hydrogen Energy* **2023**. [CrossRef]
69. Schneider, S.; Bajohr, S.; Graf, F.; Kolb, T. State of the Art of Hydrogen Production via Pyrolysis of Natural Gas. *ChemBioEng Rev.* **2020**, *7*, 150–158. [CrossRef]
70. Cornejo, A. *System for the Production of Hydrogen and Graphitic Carbon*; Hazer Group Limited: Perth, Australia, 2018.
71. Chua, H.T.; Cornejo, A.; Raston, C.L.; Gao, L. *Process for Producing Hydrogen from Hydrocarbons*; Hazer Group Limited: Perth, Australia, 2020.
72. Innova Hydrogen Corp. Apparatus and Method for Producing Graphene and Hydrogen. WO2022251979A1, 18 December 2022.
73. Lee, U.D.; Yang, C.W.; Bang, B.R.; Jeong, S.H.; Gayatri, U.I.; Kwon, H.M.; Cho, C.H.; Oh, S.J. *Reactor for Producing Hydrogen and Carbon through Pyrolysis of Methane by Thermal Storage Method, and Combination Reactor Comprising Same*; Korean Institute of Industrial Technology: Cheonan-si, Republic of Korea, 2023.
74. Shanghui, T. *Catalyst for Hydrogen Production through Catalytic Cracking of Methane and Preparation Method of Catalyst*; Zhongjing Chengkang Resource Regeneration Utilization Technology Co., Ltd., 2022. Available online: https://worldwide.espacenet.com/patent/search/family/086891789/publication/CN116328774A?q=CN116328774A (accessed on 20 September 2023).
75. Xenophon, V.; Stylianos, N. *Catalytic Materials for Pyrolysis of Methane and Production of Hydrogen and Solid Carbon with Substantially Zero Atmospheric Carbon Emissions*; Verykios Xenophon, 2022. Available online: https://worldwide.espacenet.com/patent/search/family/081185890/publication/US11401163B2?q=US11401163B2 (accessed on 20 September 2023).
76. Van Geem, K.M.; Weckhuysen, B.M. Toward an e-chemistree: Materials for electrification of the chemical industry. *MRS Bull.* **2021**, *46*, 1187–1196. [CrossRef]
77. Wismann, S.T.; Engbæk, J.S.; Vendelbo, S.B.; Bendixen, F.B.; Eriksen, W.L.; Aasberg-Petersen, K.; Frandsen, C.; Chorkendorff, I.; Mortensen, P.M. Electrified methane reforming: A compact approach to greener industrial hydrogen production. *Science* **2019**, *364*, 756. [CrossRef] [PubMed]
78. Stankiewicz, A.I.; Nigar, H. Beyond electrolysis: Old challenges and new concepts of electricity-driven chemical reactors. *React. Chem. Eng.* **2020**, *5*, 1005–1016. [CrossRef]
79. Pinto, J.; Silva, V.L.M.; Silva, A.M.G.; Silva, A.M.S.; Costa, J.C.S.; Santos, L.M.N.B.F.; Enes, R.; Cavaleiro, J.A.S.; Vicente, A.A.M.O.S.; Teixeira, J.A.C. Ohmic heating as a new efficient process for organic synthesis in water. *Green Chem.* **2013**, *15*, 970–975. [CrossRef]

80. Gupta, R.; Jalan, A.; Caram, H.S.; Dankworth, D.C. Methane Pyrolysis Using Stacked Fluidized Beds with Electric Heating of Coke. U.S. Patent Application No 17/236,418, 2020.
81. New Technologies. Available online: https://www.basf.com/global/en/who-we-are/sustainability/we-produce-safely-and-efficiently/energy-and-climate-protection/carbon-management/innovations-for-a-climate-friendly-chemical-production.html (accessed on 31 August 2023).
82. Innovative Processes for Climate-Smart Chemistry. Available online: https://report.basf.com/2021/en/shareholders/basf-on-the-capital-market/methane-pyrolysis.html (accessed on 31 August 2023).
83. Bode, A. Methane Pyrolysis—A Potential New Process for Hydrogen Production without CO_2 Emission. Available online: https://www.efzn.de/fileadmin/documents/Niedersaechsische_Energietage/Vortr%C3%A4ge/2019/NET2019_FF1_04_Bode_Rev1.pdf (accessed on 31 August 2023).
84. Philibert, C. Methane Splitting and Turquoise Ammonia. Available online: https://www.ammoniaenergy.org/articles/methane-splitting-and-turquoise-ammonia/ (accessed on 31 August 2023).
85. Fedorov, S.S.; Gubynskyi, M.V.; Livitan, M.V.; Barsukov, I.V.; Barsukov, M.G.; Wells, B.S.; Rohatgi, U.S.; Gogotsi, O.G. Ultra-High Temperature Continuous Reactors based on Electro-thermal Fluidized Bed Concept. Available online: https://asmedigitalcollection.asme.org/fluidsengineering/article-abstract/138/4/044502/374335/Ultrahigh-Temperature-Continuous-Reactors-Based-on?redirectedFrom=fulltext (accessed on 10 February 2022).
86. Gubynskyi, M.V.; Barsukov, I.V.; Gogotsi, O.G.; Fedorov, S.S.; Livitan, M.V.; Rohatgi, U. Electrothermal Fluidized Bed Furnace for Thermal Treatment of Recycled Battery Wastes. In Proceedings of the ASME 2013 Fluids Engineering Division Summer Meeting, Incline Village, NV, USA, 7–11 July 2013.
87. Volodymyrovych, H.M.; Serhiiovych, F.S.; Mykolaivna, F.S.; Vasyliovych, L.M.; Andriivna, S.T. *Electrothermal Furnace with Fluidized Bed*; National Metallurgical Academy of Ukraine: Dnipro, Ukraine, 2015.
88. Veryasov, G.; Nesterenko, N.; Vermeiren, W. Process to Conduct an Endothermic Steam Reforming Reaction in a Fluidized Bed Reactor. U.S. Patent Application No 18/017,362, 2022.
89. Veryasov, G.; Nesterenko, N.; Vermeiren, W. Process to Conduct Endothermic Direct Pyrolysis of Methane in a Fluidized Bed Reactor. U.S. Patent Application No 18/017,360, 2022.
90. Tuot, J. *The Electrothermal Fluidized Bed and Its Application to the Production of Titanium Carbide*; McGill University: Montreal, QC, Canada, 1976.
91. Manieh, A.A.; Scott, D.S.; Spink, D.R. Electrothermal fluidized bed chlorination of zircon. *Can. J. Chem. Eng.* **1974**, *52*, 507–514. [CrossRef]
92. Johnson, P.H. *Electrothermic Fluidized Bed Process*; Phillips Petroleum Co: Bartlesville, OK, USA, 1970.
93. Dietz, P.W. Electrofluidized Bed Mechanics. MIT: Cambridge, MA, USA, 1976.
94. Dong, Q.; Yao, Y.; Cheng, S.; Alexopoulos, K.; Gao, J.; Srinivas, S.; Wang, Y.; Pei, Y.; Zheng, C.; Brozena, A.H.; et al. Programmable heating and quenching for efficient thermochemical synthesis. *Nature* **2022**, *605*, 470–476. [CrossRef]
95. Dadsetan, M.; Khan, M.F.; Salakhi, M.; Bobicki, E.R.; Thomson, M.J. CO_2-free hydrogen production via microwave-driven methane pyrolysis. *Int. J. Hydrogen Energy* **2023**, *48*, 14565–14576. [CrossRef]
96. Dadsetan, M.; Latham, K.G.; Khan, M.F.; Zaher, M.H.; Manzoor, S.; Bobicki, E.R.; Titirici, M.M.; Thomson, M.J. Characterization of carbon products from microwave-driven methane pyrolysis. *Carbon Trends* **2023**, *12*, 100277. [CrossRef]
97. Hamzehlouia, S.; Chaouki, J. *Microwave-Assisted Catalytic Reactions Using Modified Bed Particles*; Polyvalor: Montreal, QC, Canada, 2018.
98. Rudolph, C.; Atakan, B. Pyrolysis of Methane and Ethane in a Compression–Expansion Process as a New Concept for Chemical Energy Storage: A Kinetic and Exergetic Investigation. *Energy Technol.* **2021**, *9*, 2000948. [CrossRef]
99. Guil-Lopez, R.; Botas, J.A.; Fierro, J.L.G.; Serrano, D.P. Comparison of metal and carbon catalysts for hydrogen production by methane decomposition. *Appl. Catal. A: Gen.* **2011**, *396*, 40–51. [CrossRef]
100. Harris, P.J.F.; Liu, Z.; Suenaga, K. Imaging the atomic structure of activated carbon. *J. Phys. Condens. Matter* **2008**, *20*, 362201. [CrossRef]
101. Kreuger, T.; van Swaaij, W.P.M.; Kersten, S.R.A. Methane pyrolysis over porous particles. *Catal. Today* **2023**, *420*. [CrossRef]
102. Philibert, C. *Methane Splitting and Turquoise Ammonia*; Ammonia Energy Association: New York, NY, USA, 2020.
103. Daloz, W.; Scheiff, F.; Ehrhardt, K.; Flick, D.; Bode, A. The quest for CO_2-free hydrogen—Methane pyrolysis at scale. In Proceedings of the ARPA-E Methane Cohort Kickoff, Houston, TX, USA, 9–10 December 2019.
104. Vander Wal, R.; Makiesse Nkiawete, M. Carbons as Catalysts in Thermo-Catalytic Hydrocarbon Decomposition: A Review. *C* **2020**, *6*, 23. [CrossRef]
105. Muradov, N.Z. CO_2-free production of hydrogen by catalytic pyrolysis of hydrocarbon fuel. *Energy Fuels* **1998**, *12*, 41–48. [CrossRef]
106. Yang, Z.; Gao, W. Applications of Machine Learning in Alloy Catalysts: Rational Selection and Future Development of Descriptors. *Adv. Sci.* **2022**, *9*, 2106043. [CrossRef]
107. Yang, L.; Liu, F.; Liu, Y.; Quan, W.; He, J. Deep regeneration of activated carbon catalyst and autothermal analysis for chemical looping methane thermo-catalytic decomposition process. *Int. J. Hydrogen Energy* **2018**, *43*, 17633–17642. [CrossRef]
108. Adamska, A.; Malaika, A.; Kozłowski, M. Carbon-Catalyzed Decomposition of Methane in the Presence of Carbon Dioxide. *Energy Fuels* **2010**, *24*, 3307–3312. [CrossRef]

109. Abbas, H.F.; Daud, W.M.A.W. An experimental investigation into the CO_2 gasification of deactivated activated-carbon catalyst used for methane decomposition to produce hydrogen. *Int. J. Hydrogen Energy* **2010**, *35*, 141–150. [CrossRef]
110. Abbas, H.F.; Daud, W.M.A.W. Thermocatalytic decomposition of methane for hydrogen production using activated carbon catalyst: Regeneration and characterization studies. *Int. J. Hydrogen Energy* **2009**, *34*, 8034–8045. [CrossRef]
111. Dufour, A.; Celzard, A.; Fierro, V.; Broust, F.; Courson, C.; Zoulalian, A.; Rouzaud, J.N. Catalytic conversion of methane over a biomass char for hydrogen production: Deactivation and regeneration by steam gasification. *Appl. Catal. A Gen.* **2015**, *490*, 170–180. [CrossRef]